Fourier Monte Carlo renormalization-group approach to crystalline membranes

A. Tröster*

Vienna University of Technology, Institute of Material Chemistry, Getreidemarkt 9, A-1060 Wien, Austria

(Received 3 October 2014; revised manuscript received 25 January 2015; published 23 February 2015)

The computation of the critical exponent η characterizing the universal elastic behavior of crystalline membranes in the flat phase continues to represent challenges to theorists as well as computer simulators that manifest themselves in a considerable spread of numerical results for η published in the literature. We present additional insight into this problem that results from combining Wilson's momentum shell renormalization-group method with the power of modern computer simulations based on the Fourier Monte Carlo algorithm. After discussing the ideas and difficulties underlying this combined scheme, we present a calculation of the renormalization-group flow of the effective two-dimensional Young modulus for momentum shells of different thickness. Extrapolation to infinite shell thickness allows us to produce results in reasonable agreement with those obtained by functional renormalization group or by Fourier Monte Carlo simulations in combination with finite-size scaling. Moreover, our method allows us to obtain a decent estimate for the value of the Wegner exponent ω that determines the leading correction to scaling, which in turn allows us to refine our numerical estimate for η previously obtained from precise finite-size scaling data.

DOI: 10.1103/PhysRevE.91.022132 PACS number(s): 64.60.De, 05.10.Ln, 46.70.Hg, 05.70.Jk

I. INTRODUCTION

The paradigm of the renormalization group (RG) is without doubt a cornerstone of modern theoretical physics with countless applications, and it has been enormously influential in many areas of science beyond its origins rooted in high-energy physics and statistical mechanics [1]. Indeed, the abstract RG concept may be regarded as a cleverly organized successive divide-and-conquer strategy to deal with problems that involve a large number of mutually coupled degrees of freedom. However, concrete applications of an RG scheme may superficially appear to look very different from one another. In the present article, we will concentrate on Wilson's momentum shell RG (MSRG) approach to the field-theoretic formulation of critical phenomena at second-order phase transitions [2]. The MSRG is certainly an invaluable conceptual tool both for abstract reasoning as well as in a first qualitative or even semiquantitative analysis of a given problem. In a nutshell, one writes the underlying Hamiltonian in terms of Fourier amplitudes $\tilde{f}(\boldsymbol{k})$ of the underlying fields. Imposing a wave-vector cutoff Λ, one tries to identify an effective Hamiltonian as it would emerge after having integrated out all microscopic degrees of freedom that describe the physics of the system below scales of size $1/\Lambda$. In this effective Hamiltonian, only those couplings are kept that are regarded as important in the long-wavelength limit, while the effect of all other couplings that are related to the eliminated short-ranged degrees of freedom is absorbed into an assumed renormalization of these surviving couplings. The fact that the choice of the cutoff Λ is arbitrary suggests to iterate this prescription as follows. The effects of the "fastest" degrees of freedom that reside in a momentum shell $\Lambda/b < |\boldsymbol{k}| \leqslant \Lambda, b > 1$ beneath the cutoff Λ are successively integrated out from the partition function, which gives rise to a yet another set of modified coupling constants. On properly rescaling lengths and "renormalizing" the field, one derives a flow pattern in the space of coupling constants. An analysis of the fixed points (FPs) of this flow then allows us to explain the phenomenon of universality and to extract numerical values for the critical exponents. Unfortunately, concrete analytical implementations of this program usually rely on some type of perturbative approximation, and calculations frequently become intractable beyond one loop order. Thus, for actual numerical calculations, other approaches such as the field-theoretic RG [3] or the functional RG [4] are preferred, or one resorts to real-space computer simulations in combination with finite-size scaling (FSS) [5,6].

For the task of implementing Wilson's MSRG scheme in a simulation, real-space MC approaches are obviously not very well suited. On the other hand, our Fourier Monte Carlo algorithm (FMC) [7–11] is tailor-made for this problem. Recently, we have demonstrated that it allows us to follow the MSRG prescription step by step in simulation [12,13]. This is quite appealing, as it eliminates the perturbative approximations and the underlying need for a "small parameter" from the concrete application of the MSRG, thus representing a truly nonperturbative implementation. On the other hand, as in any humanly possible MSRG calculation, one is still forced to project the calculated RG flow from its native infinite-dimensional coupling space to a suitable low-dimensional subspace spanned by a finite number of effective coupling parameters. Even though no perturbative approximation is involved, the presence of this inevitable projection, which amounts to ignoring the effects of the remaining directions in the space of coupling constants, may do substantial harm to the achieved numerical precision.

Inspired by early analytic work by Bruce, Droz, and Aharony [14], subsequent work [13,15] indicates that by optimizing the results with respect to the parameter b that governs the thickness of the momentum shell (we will discuss below in more detail how this works), MSRG can indeed be turned from a qualitatively to a quantitatively useful tool. To date, this has only been demonstrated for a particularly convenient model system, namely the long-ranged Ising model of Fisher, Ma, and Nickel [16]. One purpose of the present paper is to test the ideas put forward in Refs. [13,15] on a

*andreas.troester@tuwien.ac.at

nontrivial real-world problem, namely the elastic behavior of crystalline membranes in the flat phase. It is well known [17] that the corresponding universal behavior of long-wavelength fluctuations is governed by a single exponent η. However, as noted in Ref. [18], a glance at the existing literature reveals a considerable spread of numerical results for η, obtained from a variety of analytical approaches such as, e.g., self-consistent field theory [19,20], ϵ expansion [21], large d expansion [22], and functional RG [23–25], or from simulation approaches derived in real space (see, e.g., Refs. [26,27]). In our own simulations (Ref. [18]), which are based on our Fourier MC algorithm in combination with FSS, we have noticed a rather strong influence of corrections to scaling, which indicates the importance of properly taking into account the role of RG-irrelevant couplings if one aims at high numerical precision. Interestingly, up to now nobody seems to have succeeded in deriving a numerical estimate of the exponent ω governing the corrections to scaling (cf. [28]) of a crystalline membrane in its flat phase. It is the second goal of the present paper to provide such a numerical estimate.

II. A DIFFERENT VIEW ON STANDARD MSRG

As explained in the Introduction, MSRG is a fairly standard method. However, for the convenience of the reader, we will summarize the main steps, emphasizing those aspects that are particularly relevant to our present approach. A MSRG transformation can be performed on an arbitrary Hamiltonian $\mathcal{H}^{\Lambda}_{\boldsymbol{K}}[f]$ formulated in terms of the Fourier amplitudes $\tilde{f}(\boldsymbol{k})$ of a field $f(\boldsymbol{x})$ defined for wave vectors of moduli up to a chosen momentum space cutoff Λ. The formal vector $\boldsymbol{K}$ holds all "coupling constants" that are admissible for the symmetry constraints imposed on the underlying system. Let $\mathcal{K}$ denote the infinite-dimensional space of all such coupling vectors. One chooses a shell thickness parameter $b > 1$ and splits the Fourier amplitudes $\tilde{f}(\boldsymbol{k}) \equiv \tilde{f}_<(\boldsymbol{k}) + \tilde{f}_>(\boldsymbol{k})$ into "slow" and "fast" contributions,

$$\tilde{f}_<(\boldsymbol{k}) = \theta(\Lambda/b - |\boldsymbol{k}|)\tilde{f}(\boldsymbol{k}), \tag{1}$$

$$\tilde{f}_>(\boldsymbol{k}) = \theta(|\boldsymbol{k}| - \Lambda/b)\tilde{f}(\boldsymbol{k}), \tag{2}$$

where θ denotes the Heaviside step function. Functional integration over the fast modes

$$e^{-\tilde{\mathcal{H}}^{\Lambda/b}_{\tilde{\boldsymbol{K}}}[f_<]} \equiv \int \mathcal{D}f_> e^{-\mathcal{H}^{\Lambda}_{\boldsymbol{K}}[f_<+f_>]} \tag{3}$$

then yields a coarse-grained Hamiltonian for the remaining slow modes and induces a mapping $\boldsymbol{K} \to \tilde{\boldsymbol{K}}$. This coarse-graining step is followed by a rescaling $\boldsymbol{k}' = b\boldsymbol{k}$ of "momenta" (i.e., inverse length) scales and restoration of the original cutoff Λ. Finally, one performs a renormalization

$$\tilde{f}_<(\boldsymbol{k}'/b) = z(b,\boldsymbol{K})f'(\boldsymbol{k}') \tag{4}$$

of field amplitudes with

$$z(b,\boldsymbol{K}) = b^{d-[f]-\frac{\eta[\boldsymbol{K}]}{2}}. \tag{5}$$

Here, d is the spatial dimension, $[f]$ is the canonical momentum dimension of f, and the so-called anomalous dimension $\eta[\boldsymbol{K}]/2$ is a function that characterizes the specific FP to be investigated (see below). For the example of a coupling constant C multiplying a monomial containing n powers of the field f and p spatial derivatives in the effective Hamiltonian, it is straightforward to show that the coarse-grained coefficient $\tilde{C}$ undergoes a total rescaling,

$$C' = b^{[C]-n\frac{\eta[\boldsymbol{K}]}{2}}\tilde{C}, \tag{6}$$

where p is implicitly accounted for in the canonical momentum dimension $[C] = d - n[f] - p$.

Consecutive application of these three steps induces a mapping $\tilde{\boldsymbol{K}} \to \boldsymbol{K}'$, which defines the RG transformation $\mathcal{R}_b : \mathcal{K} \to \mathcal{K}$. The crux of the whole construction is the observation that as a result of the rescaling operation, the correlation lengths of systems at $\boldsymbol{K}$ and $\boldsymbol{K}'$ are related by $\xi[\boldsymbol{K}'] = \xi[\boldsymbol{K}]/b$. At a FP $\boldsymbol{K}^* = \mathcal{R}_b(\boldsymbol{K}^*)$, this leaves only the possibility of an infinite or zero correlation length. Each such FP characterizes a different universality class of critical behavior, and nontrivial behavior is, of course, found for infinite correlation length.

In principle, the operation $\mathcal{R}_b$ can be defined for any $b > 1$, and it satisfies the eponymous semigroup property

$$\mathcal{R}_{b_1 b_2} = \mathcal{R}_{b_1} \circ \mathcal{R}_{b_2}, \tag{7}$$

where "$\circ$" denotes composition of maps, which is paramount to the emergence of power laws that dominate the subsequent analysis as well as to the independence of the associated exponent values of the particular choice of the shell thickness parameter b. In the vicinity of $\boldsymbol{K}^*$ where $\mathcal{R}_b$ can be linearized, most directions in the space $\mathcal{K}$ turn out to be exponentially attractive ("irrelevant"), while typically only one or two are exponentially repulsive ("relevant"), and thus must be carefully tuned to "reach" the FP $\boldsymbol{K}^*$ under successive iteration of $\mathcal{R}_b$. Ultimately, this explains the observed universality of critical phenomena. The RG flow resulting from the above scheme is defined in the infinite-dimensional coupling constant space $\mathcal{K}$. In practical calculations, we are nevertheless forced to limit ourselves to working with *effective* Hamiltonians, i.e., Hamiltonians $\mathcal{H}^{\Lambda}_{\boldsymbol{K}_{\rm eff}}[f]$ that are parametrized exclusively by coupling vectors $\boldsymbol{K}_{\rm eff} \in \mathcal{K}_{\rm eff}$ taken from a low-dimensional linear subspace $\mathcal{K}_{\rm eff} \subset \mathcal{K}$ of dimension, say, $d_{\rm eff}$, spanned by the relevant and the least irrelevant directions with respect to the FP $\boldsymbol{K}^*$. In terms of suitably chosen coordinates in the space $\mathcal{K}$, the projection $\pi_{\rm eff} : \mathcal{K} \to \mathcal{K}_{\rm eff}$ onto this finite-dimensional space assumes the form

$$\pi_{\rm eff}(K_1, K_2, \dots) = (K_1, K_2, \dots K_{d_{\rm eff}}, 0, 0, \dots). \tag{8}$$

Except for trivial cases, $\mathcal{K}_{\rm eff}$ is not an invariant subspace under the action of $\mathcal{R}_b$, i.e., $\mathcal{R}_b$ and $\pi_{\rm eff}$ do not commute, because "new" couplings are inevitably generated from a generic effective Hamiltonian under the coarse-graining operation, regardless of our ability to perform the coarse-graining operation exactly or by some approximate method. If the subspace $\mathcal{K}_{\rm eff} \subset \mathcal{K}$ has been chosen properly, the "missing" directions will only correspond to strongly irrelevant directions in coupling space, whose influence will be exponentially suppressed. In mathematical terms, any humanly possible MSRG calculation amounts to replacing the exact RG transformation $\mathcal{R}$ by the effective transformation

$$\mathcal{R}^{\rm eff}{}_b := \pi_{\rm eff} \circ \mathcal{R}_b \circ \pi_{\rm eff}. \tag{9}$$

The crucial observation is, however, that, in contrast to $\mathcal{R}_b$, the effective transformations ${\mathcal{R}^{\text{eff}}}_b$ do *not* strictly form a half-group, i.e.,

$$ {\mathcal{R}^{\text{eff}}}_{b_1 b_2} \neq {\mathcal{R}^{\text{eff}}}_{b_1} \circ {\mathcal{R}^{\text{eff}}}_{b_2}, \tag{10} $$

since in the composite operation on the right side the additional irrelevant couplings generated by ${\mathcal{R}^{\text{eff}}}_b$ will be "lost" in the subsequent application of π_{eff}. Of course, nothing can prevent us from studying iterations of the map ${\mathcal{R}^{\text{eff}}}_b$ in a manner similar to $\mathcal{R}_b$. The harm that the failure of ${\mathcal{R}^{\text{eff}}}_b$ to close under composition causes to the subsequent analysis depends on the "production rate" of coupling components generated during the coarse-graining step that fall outside of $\mathcal{K}_{\text{eff}}$, which in turn is controlled by the shell thickness parameter b. In particular, the projection $\pi_{\text{eff}}(\boldsymbol{K}^*)$ of the "true" infinite-dimensional FP $\boldsymbol{K}^*$ of $\mathcal{R}_b$ generally *does not* produce a FP of ${\mathcal{R}^{\text{eff}}}_b$. Instead, the locations of FPs ${\boldsymbol{K}_{\text{eff}}}^* = {\boldsymbol{K}_{\text{eff}}}^*(b) \in \mathcal{K}_{\text{eff}}$ of the transformations ${\mathcal{R}^{\text{eff}}}_b$ will generally be *b-dependent*. Furthermore, the same is true for the numerical values of critical exponents calculated from a linearization of ${\mathcal{R}^{\text{eff}}}_b$ around ${\boldsymbol{K}_{\text{eff}}}^*(b)$.

In summary, even though the results of the exact RG prescription in infinite-dimensional coupling space $\mathcal{K}$ are guaranteed to be independent of the arbitrary parameter b, the projection π_{eff} to the low-dimensional space $\mathcal{K}_{\text{eff}}$ introduces such a b dependence that encodes the effects of the remaining irrelevant directions. While this seems to look pathological at first glance, it actually allows us to optimize the resulting calculation scheme by determining the value b^* at which the drift of $\boldsymbol{K}_{\text{eff}}(b)$ becomes stationary. In this respect, our philosophy is similar to that of other approaches in which an arbitrary parameter is introduced whose value would drop out of the results of exact theory but nevertheless may be used to optimize an approximated version. A nice example illustrating the power of such a strategy is Kleinert's "variational perturbation theory" [29]. However, it is very important to keep in mind that the present b-related "pathologies" are *nonperturbative* in the sense that they do not originate from the use of any perturbative approximation in evaluating the CG step, but purely arise from the necessity to limit ourselves to considering a finite number of couplings in a real-world calculation. Amusingly, these effects are neither noticed in standard perturbative MSRG calculations (where it is extremely convenient to consider momentum shells that are infinitesimally thin, since in the limit $\Delta b := b - 1 \to 0_+$ the appearing Feynman integrals are usually much easier to evaluate than for finite Δb) nor in most popular real-space RG schemes, where the value of b is usually dictated by the decimation scheme chosen for the given lattice topology. In fact, it is difficult to find any papers that use momentum shells of finite thickness for anything beyond qualitative arguments. One notable exception is the work of Bruce, Droz, and Aharony [14], who argued that the influence of irrelevant couplings in perturbative calculations of the exponents of a standard short-ranged Landau-Ginzburg (LG) model should be greatly diminished in the limit of large b. And indeed, notice that $b^* \to \infty$ and $b^* \to 1$ are the only values of b^* that allow us to reconcile the expected b-dependent features discussed above with the validity of the usual semigroup property $\mathcal{R}_{b^{*2}} = \mathcal{R}_{b^*} \circ \mathcal{R}_{b^*}$.

Our recently developed FMC method is nonperturbative by definition and necessarily uses momentum shells of finite thickness, since our simulations are done for a finite lattice of linear size L with lattice constant $a = 1$, which implies a minimum spacing of $\Delta k_i = 2\pi/L$ between components of adjacent wave vectors. Thus, it is perfectly suited to study the b dependence of ${\mathcal{R}^{\text{eff}}}_b$ and check the predictions of Bruce *et al.* that had been derived with the use of the ϵ expansion. Of course, due to the discrete nature of the Brillouin zones of our finite systems, neither the limit $b \to 1$ nor the limit $b \to \infty$ are directly accessible, but we can monitor or even try to extrapolate the behavior of the corresponding observables towards these limits.

For the purpose of putting our ideas to the test, the short-range LG model used in Ref. [14] is not very suitable in view of the numerical smallness of its exponent, $\eta = \epsilon^2/54 + O(\epsilon^3)$. Instead, in Ref. [15] we considered the long-range generalization of the LG model introduced by Fisher, Ma, and Nickel in Ref. [16]. This model was particularly convenient since the exponent η of its Wilson-Fisher FP is exactly known, thus saving the numerical effort to determine it numerically from the simulation data. In addition, detailed analytical calculations and quite precise Monte Carlo data were available for comparison [30]. Using our FMC implementation of MSRG, we were indeed able to observe the b dependence of ${\boldsymbol{K}_{\text{eff}}}^*(b)$ and its associated exponents. However, contrary to our initial expectations, it turned out that the best accuracy was not obtained in the large-b limit. Instead, for varying b, the FP $b \mapsto {\boldsymbol{K}_{\text{eff}}}^*(b)$ moves along a "trajectory" in the plane $\mathcal{K}_{\text{eff}}$ that exhibits a turning point at a certain shell thickness b^* that was actually found to be rather close to but distinct from $b = 1$, and for this distinguished value b^* we observed that the values of the critical exponents ν and ω were in excellent agreement with the benchmark results derived in Ref. [30]. A systematic study for different system sizes revealed the surprising discovery that $1 < b^* < \infty$ is not a finite-size effect. Nevertheless, we speculate that this peculiar finding is highly specific to the model of Fisher, Ma, and Nickel, and we still expect that usually $b^* \to 1$ or $b^* \to \infty$ will instead be found in other systems. The rest of the paper will therefore be devoted to the application of our ideas to a real-world system, whose critical properties are still an active area of research: the elastic behavior of crystalline membranes.

III. FMC IMPLEMENTATION OF MSRG FOR CRYSTALLINE MEMBRANES

As explained in detail in Refs. [17,31], the flat phase of a crystalline membrane is conveniently described in the so-called Monge parametrization, which amounts to specifying a scalar "height" function $f(x)$ that measures the out-of-plane deformations of the membrane with respect to a two-dimensional reference plane, which we take to be of size $L \times L$ with periodic boundary conditions understood. The long-wavelength physics of the system is captured by the Fourier modes

$$ \tilde{f}(\boldsymbol{q}) = \theta(\Lambda - |\boldsymbol{q}|) \int d^2x f(\boldsymbol{x}) e^{-i\boldsymbol{q}\cdot\boldsymbol{x}}, \tag{11} $$

where the Heaviside step function is used to impose a cutoff Λ in the space of wave vectors. Formally embedding the vectors $\boldsymbol{q}, \boldsymbol{Q}$ in $\mathbb{R}^3$ and abbreviating $\widehat{\boldsymbol{Q}} = \boldsymbol{Q}/|\boldsymbol{Q}|$, we define

$$\tilde{\mathcal{F}}(\boldsymbol{Q}) = \int \frac{d^2q}{(2\pi)^2} \left(\widehat{\boldsymbol{Q}} \times \boldsymbol{q}\right)^2 \tilde{f}(\boldsymbol{q})\tilde{f}(\boldsymbol{Q}-\boldsymbol{q}). \tag{12}$$

In terms of this generalized convolution, the effective Hamiltonian that describes the universal properties of the flat phase at long wavelengths is given by

$$\mathcal{H}^{\Lambda}[f] = \frac{\kappa}{2}\int \frac{d^2q}{(2\pi)^2} q^4 |\tilde{f}(\boldsymbol{q})|^2 + \frac{K}{8}\int \frac{d^2Q}{(2\pi)^2} |\tilde{\mathcal{F}}(\boldsymbol{Q})|^2. \tag{13}$$

Its first contribution, the bending energy, is represented by a local dispersion term as found in a standard LG model, except that the usual gradient term $(\nabla f)^2$ is replaced by a Laplacian $(\Delta f)^2$. In addition, while its second contribution also involves four powers of f, the nonlocal characteristic of the generalized convolution (12) hints at physics that is quite different from that of the standard LG model. As discussed in Refs. [17,32], this nonlocality encodes an effective long-range anharmonic self-interaction of the out-of-plane deformations f mediated by in-plane phonons that had been integrated out in the calculation steps leading to (13). $\mathcal{H}[f]$ involves only two coupling constants, namely the bending stiffness κ and the the effective two-dimensional (2D) Young modulus $K = 4\mu(\mu+\lambda)/(2\mu+\lambda)$ composed from the in-plane Lame constants λ and μ of the membrane. Implicit in all these constants as well as in the formulas (13) but suppressed in our present notation is a dependence on the cutoff Λ.

To implement our FMC algorithm, we replace the membrane reference plane by a square $L \times L$ lattice with $N = L^2$ sites and lattice constant $a = 1$, and we keep the imposed periodic boundary conditions. Assuming L to be even without loss of generality, we may parametrize wave vectors inside the full first Brillouin zone of this lattice by $q_i = 2\pi m_i/L$, $m_i = -L/2+1,\ldots,0,\ldots,L/2$, and the above integrals over the Brillouin zone are replaced by finite sums. In view of the rectangular structure of the underlying lattice, it is natural to replace spherical cutoffs Λ that are convenient in analytic continuum calculations by a more suitable cubic version. Parametrized by an integer l, in our simulation a cutoff $\Lambda = 2\pi l/L$ is applied to each separate wave-vector component, and in order to avoid problems with "umklapp" terms and minimize the effects of lattice anisotropy, it is recommended to choose $l \ll L/2$. To implement the coarse-graining step in FMC, we furthermore choose an inner cutoff $\Lambda' = 2\pi l'/L$ with $0 < l' < l$. The shell thickness parameter is then given by $b = \Lambda/\Lambda' = l/l'$.

The discrete Fourier transform convention

$$\tilde{f}(\boldsymbol{q}) = \begin{cases} \sum_{\boldsymbol{x}} f(\boldsymbol{x}) e^{-i\boldsymbol{q}\cdot\boldsymbol{x}}, & |q_i| < \Lambda, \\ 0, & \text{otherwise} \end{cases} \tag{14}$$

with inversion

$$f(\boldsymbol{x}) = \frac{1}{N}\sum_{|q_i|<\Lambda} \tilde{f}(\boldsymbol{q}) e^{i\boldsymbol{q}\cdot\boldsymbol{x}}, \tag{15}$$

in which the Fourier amplitudes are extensive quantities, may look somewhat asymmetric. It proves to be convenient in comparing discrete to continuous formulas. Since the membrane's elastic free energy does not depend on the average distance of the membrane to the Monge reference plane but merely on variations of its height, only derivatives of f enter in the continuum formulation (13). Therefore, we can further assume without loss of generality that $\tilde{f}(\boldsymbol{0}) = 0$. In terms of these discrete amplitudes, the above formulas (12) and (13) are replaced by

$$\tilde{\mathcal{F}}(\boldsymbol{Q}) = \sum_{\boldsymbol{q}} \left(\widehat{\boldsymbol{Q}} \times \boldsymbol{q}\right)^2 \tilde{f}(\boldsymbol{q})\tilde{f}(\boldsymbol{Q}-\boldsymbol{q}) \tag{16}$$

and

$$\mathcal{H}^{\Lambda}[f] = \frac{\kappa_N}{2}\sum_{\boldsymbol{q}\neq\boldsymbol{0}} q^4 |\tilde{f}(\boldsymbol{q})|^2 + \frac{K_N}{8}\sum_{\boldsymbol{Q}\neq\boldsymbol{0}} |\tilde{\mathcal{F}}(\boldsymbol{Q})|^2, \tag{17}$$

where

$$\kappa_N = \frac{\kappa}{N}, \quad K_N = \frac{K}{N^3}. \tag{18}$$

In view of the extensive discussions already available in the literature (cf. Refs. [8,10,33,34]) and the detailed layout of the specific implementation for the case of crystalline membranes presented in the companion paper [18], we would like to keep the description of the basic Fourier Monte Carlo algorithm and its general properties at a minimum in the present paper. However, it turns out that setting up the coarse-graining step of MSRG for a crystalline membrane requires us to define different MC moves for slow and fast modes of the so-called "tracer" configurations to be defined below. In the standard cubic FMC scheme, the momentum shell corresponding to a prescribed pair of cutoffs $\Lambda' < \Lambda$ is, of course, defined as the set of wave vectors with components $p_i, i = 1,2$ subject to the constraints $|p_i| \leqslant \Lambda$ and $\max_i |p_i| > \Lambda'$. MC moves of fast modes $\tilde{f}_>(\boldsymbol{q})$ are performed by picking a random wave vector $\boldsymbol{p}$ from this shell, choosing a random complex number inside a circle $|\epsilon| < \rho$ of radius ρ around 0 in the complex plane, and considering the shift

$$\tilde{f}(\boldsymbol{q}) \to \tilde{f}(\boldsymbol{q}) + \epsilon\delta_{\boldsymbol{q},\boldsymbol{p}} + \epsilon^*\delta_{\boldsymbol{q},-\boldsymbol{p}}. \tag{19}$$

Taking advantage of the special convoluted structure (12) of the anharmonic term appearing in (13), it is then possible to calculate the resulting change in energy in an efficient way, as is explained in detail in Ref. [18].

Integrating out these fast modes by means of an FMC simulation should then produce a coarse-grained Hamiltonian of general structure,

$$\tilde{\mathcal{H}}^{\Lambda/b}[f] = \frac{1}{2}\sum_{\boldsymbol{q}} [\tilde{\kappa}_N q^4 + \cdots]|\tilde{f}(\boldsymbol{q})|^2 + \frac{1}{8}\sum_{\boldsymbol{Q}} [\tilde{K}_N + \cdots]|\tilde{\mathcal{F}}(\boldsymbol{Q})|^2 + O(f^6), \tag{20}$$

with

$$\tilde{\mathcal{F}}(\boldsymbol{Q}) = \sum_{\boldsymbol{q}} (\widehat{\boldsymbol{Q}} \times \boldsymbol{q})^2 \tilde{f}(\boldsymbol{q})\tilde{f}(\boldsymbol{Q}-\boldsymbol{q}), \tag{21}$$

from which we wish to extract the two CG relations $\kappa_N \mapsto \tilde{\kappa}_N$ and $K_N \to \tilde{K}_N$, i.e., $\kappa \mapsto \tilde{\kappa}$ and $K \to \tilde{K}$. For this purpose, we determine the value of the CG Hamiltonian (20) by restricting the MC sampling to certain "tracer configurations" defined by

a particularly simple and convenient choice of their slow mode parts. In terms of simplicity, our preferred type of such a tracer configuration would certainly be that of an isolated "dumbbell" of just two slow modes with a common uniform real-valued amplitude at the fixed wave vector $\pm\boldsymbol{k}$. This dumbbell is surrounded by the shell of nonzero fast modes, but all other slow modes are set to zero. In formal terms, the slow parts of such dumbbell tracer configurations $\tilde{f}^{(\boldsymbol{k})}(\boldsymbol{q})$ defined with respect to $\pm\boldsymbol{k}$ are restricted to be of the type

$$\tilde{f}^{(\boldsymbol{k})}_{<}(\boldsymbol{q}) \equiv f_d(\delta_{\boldsymbol{q}-\boldsymbol{k}} + \delta_{\boldsymbol{q}+\boldsymbol{k}}),\ f_d \in \mathbb{R}\,. \tag{22}$$

As explained in detail in Refs. [7,8], for this class of tracer configurations one now performs a multicanonical type of simulation of, e.g., the Wang-Landau type, in which the probability distribution $P(f_d)$ of the "reaction coordinate" f_d in the "bath" of fast modes is calculated. A polynomial fit of $-\ln P(f_d)$ then yields a set harmonic and lowest-order anharmonic coefficients $a_2(\boldsymbol{k}),a_4(\boldsymbol{k}),\ldots$ for each chosen wave vector $\boldsymbol{k}$. A comparison of these coefficients with the general $\boldsymbol{k}$-dependent structure of the bare effective Hamiltonian then allows us to determine a "new" set of bare parameters. In other words, one obtains all the information required for completing the coarse-graining step of the MSRG prescription.

For LG-type models with a local anharmonic energy contribution, this class of tracer configuration allows us to determine the flow of coupling parameters. Unfortunately, however, for our present problem the dumbbell class (22) is insufficient to capture the flow of the anharmonic part of the bare Hamiltonian. In fact, in the formula

$$\tilde{\mathcal{F}}^{(\boldsymbol{k})}_{<}(\boldsymbol{Q}) = (\hat{\boldsymbol{Q}} \times \boldsymbol{k})^2[\delta_{\boldsymbol{Q}-2\boldsymbol{k}} + 2\delta_{\boldsymbol{Q}} + \delta_{\boldsymbol{Q}+2\boldsymbol{k}}]f_d^2 \tag{23}$$

that results for amplitudes $\tilde{\mathcal{F}}(\boldsymbol{Q})$ built exclusively from the slow part $\tilde{f}^{(\boldsymbol{k})}_{<}(\boldsymbol{q}) = f_d(\delta_{\boldsymbol{q}-\boldsymbol{k}} + \delta_{\boldsymbol{q}+\boldsymbol{k}})$, the vector $\boldsymbol{Q}$ is constrained to be either zero (which is forbidden) or parallel to $\boldsymbol{k}$, in which case the leading cross product vanishes, i.e., $\tilde{\mathcal{F}}^{(\boldsymbol{k})}_{<}(\boldsymbol{Q}) \equiv 0$. To overcome this difficulty, we instead consider a "cross" tracer configuration with slow parts of the type

$$\tilde{f}^{\boldsymbol{k}}_{<}(\boldsymbol{q}) = f_c(\delta_{\boldsymbol{q}-\boldsymbol{k}} + \delta_{\boldsymbol{q}-\boldsymbol{k}^\perp} + \delta_{\boldsymbol{q}+\boldsymbol{k}} + \delta_{\boldsymbol{q}+\boldsymbol{k}^\perp}), \tag{24}$$

where $f_c \in \mathbb{R}$ and $|\boldsymbol{k}| = |\boldsymbol{k}^\perp|, \boldsymbol{k}\cdot\boldsymbol{k}^\perp = \boldsymbol{0}$, which map out a symmetric "cross" spanned by two orthogonal vectors $\boldsymbol{k}$ and $\boldsymbol{k}^\perp$ of equal length around $\boldsymbol{0}$ with one common real-valued amplitude, all remaining slow modes being silenced to zero. For this class of tracer configuration, a lengthy but elementary calculation yields

$$\begin{aligned}\tilde{\mathcal{F}}^{\boldsymbol{k}}(\boldsymbol{Q}) = 2(\hat{\boldsymbol{Q}} \times \boldsymbol{k})^2 f_c^2[&\delta_{\boldsymbol{Q}-\boldsymbol{k}-\boldsymbol{k}^\perp} + \delta_{\boldsymbol{Q}+\boldsymbol{k}-\boldsymbol{k}^\perp} \\ &+ \delta_{\boldsymbol{Q}-\boldsymbol{k}+\boldsymbol{k}^\perp} + \delta_{\boldsymbol{Q}+\boldsymbol{k}+\boldsymbol{k}^\perp}].\end{aligned} \tag{25}$$

In particular, if the arms of the cross are chosen to point along the directions $\boldsymbol{k} = (k,0)$, $\boldsymbol{k}^\perp = (0,k)$ of the Cartesian axes, we have

$$(\hat{\boldsymbol{Q}} \times \boldsymbol{k})^2\delta_{\boldsymbol{Q}\pm\boldsymbol{k}\pm\boldsymbol{k}^\perp} = \frac{k^2}{2}\delta_{\boldsymbol{Q}-(\pm k,\pm k)}, \tag{26}$$

and the above equation simplifies to

$$\tilde{\mathcal{F}}^{\boldsymbol{k}}(\boldsymbol{Q}) = k^2 f_c^2 \times \begin{cases} 1, & \boldsymbol{Q} = (\pm k, \pm k), \\ 0, & \text{otherwise.} \end{cases} \tag{27}$$

Using this result, we calculate the total energy contribution of a cross configuration without fast modes as

$$E^{\boldsymbol{k}}(f_c) = 2\kappa_N k^4 f_c^2 + \frac{K_N}{2}k^4 f_c^4. \tag{28}$$

From the MC point of view, (24) imposes an extra constraint on the allowed phase space in addition to the reality condition $\tilde{f}(\boldsymbol{k}) = \tilde{f}^*(-\boldsymbol{k})$ for the fast modes during the sampling. We thus need to calculate the effect of a variation,

$$\delta f(\boldsymbol{q}) = r(\delta_{\boldsymbol{q}-\boldsymbol{k}} + \delta_{\boldsymbol{q}-\boldsymbol{k}^\perp} + \delta_{\boldsymbol{q}+\boldsymbol{k}} + \delta_{\boldsymbol{q}+\boldsymbol{k}^\perp}), \tag{29}$$

of the cross configuration by the real number r on the total energy. For the harmonic contribution, it is easy to see that

$$\delta E_{\text{harm}} = 4\kappa_N k^4(rf_c + r^2/2). \tag{30}$$

It remains to calculate the change of the anharmonic contribution to the energy under a MC move (29). In terms of the shift $\delta\tilde{\mathcal{F}}(\boldsymbol{Q})$, for which a lengthy and tedious calculation yields

$$\begin{aligned}\delta\tilde{\mathcal{F}}(\boldsymbol{Q}) = 2r(\hat{\boldsymbol{Q}} \times \boldsymbol{k})^2[&\tilde{f}(\boldsymbol{Q}-\boldsymbol{k}) + \tilde{f}(\boldsymbol{Q}+\boldsymbol{k}) + r\delta_{\boldsymbol{Q}-\boldsymbol{k}-\boldsymbol{k}^\perp}] \\ &+ (\boldsymbol{k} \leftrightarrow \boldsymbol{k}^\perp),\end{aligned} \tag{31}$$

this last missing piece of information is readily obtained from the general variation formula

$$\delta E_{\text{anharm}} = \frac{K_N}{8}\sum_{\boldsymbol{Q}\neq\boldsymbol{0}}[2\tilde{\mathcal{F}}(\boldsymbol{Q})\delta\tilde{\mathcal{F}}(-\boldsymbol{Q}) + |\delta\tilde{\mathcal{F}}(\boldsymbol{Q})|^2] \tag{32}$$

valid for all types of FMC moves.

Recently [18], we introduced a variant of FMC that is able to efficiently suppress critical slowing down, i.e., exponential growth of integrated autocorrelation times in critical or nearly critical systems. This is achieved by iteratively optimizing the MC acceptance rates of individual Fourier amplitudes during the start-up phase of the simulation for each wave vector separately, aiming at acceptance rates between 30% and 40% for each amplitude. In the present simulations, such an optimization was, of course, also implemented.

In what follows, we shall assume that without loss of generality, $\kappa = 1$, such that only a dependence on the anharmonic coupling parameter K remains. The coarse-graining procedure outlined so far produces a shift

$$\boldsymbol{K} := \begin{pmatrix} 1 \\ K \end{pmatrix} \mapsto \begin{pmatrix} \tilde{\kappa} \\ \tilde{K} \end{pmatrix} =: \tilde{\boldsymbol{K}}. \tag{33}$$

According to (6), rescaling of lengths and further "wave-function" renormalization then leads to

$$\tilde{\boldsymbol{K}} \mapsto \begin{pmatrix} b^{-\eta(K)}\tilde{\kappa} \\ b^{2-2\eta(K)}\tilde{K} \end{pmatrix} =: \begin{pmatrix} \kappa' \\ K' \end{pmatrix} =: \boldsymbol{K}' \tag{34}$$

since $[\kappa] = 0$ and $[K] = 2$. A concrete RG flow $\boldsymbol{K} \to \boldsymbol{K}'$ is only defined after specifying the function $\eta(K)$. Imposing invariance $\kappa' \equiv 1$ of the harmonic dispersion term gives

$$\eta(K) = \frac{\ln\tilde{\kappa}(K)}{\ln b}, \tag{35}$$

where we explicitly indicate the dependence of $\tilde{\kappa}$ on the parameter K. On the other hand, an invariance condition $K' \equiv K$ would implicitly define a function $\eta_K(K)$ by

$$\eta_K(K) \equiv 1 + \frac{\ln\frac{\tilde{K}(K)}{K}}{2\ln b}. \tag{36}$$

At a FP $K' \equiv K \equiv K^*$, the common value

$$\eta(K^*) = \eta_K(K^*) \equiv \eta \tag{37}$$

of the two functions $\eta(K)$ and $\eta_K(K)$ is the critical exponent η. Thus K^* can be numerically determined as the location of the common intersection point of these functions plotted against K.

Since the RG transform $K \mapsto K'(K)$ is designed to be analytic, we can linearize it around the FP value K^*, such that

$$K'(K^* + \delta K) \approx K^* + \mathcal{M} \cdot \delta K, \tag{38}$$

where

$$\mathcal{M} := \left. \frac{dK'(K)}{dK} \right|_{K=K^*} \tag{39}$$

denotes the slope of the function $K \mapsto K'(K^*) - K^*$ at its zero $K = K^*$, which can readily be assessed in our simulations. For a nontrivial infrared attractive FP, we expect that K is irrelevant and thus $|\mathcal{M}| < 1$. If $K'(K)$ does not oscillate back and forth around this FP during successive RG iterations, we should also expect $\mathcal{M} > 0$. The corresponding Wegner [35] exponent ω is then defined through $\mathcal{M} \equiv b^{-\omega}$, i.e.,

$$\omega = -\frac{\ln \mathcal{M}}{\ln b}. \tag{40}$$

IV. NUMERICAL EVALUATION STRATEGY

The membrane systems studied in our simulations may be parametrized by a triple of integers (L,l,l'), such that $\Lambda = 2\pi l/L, \Lambda' = 2\pi l'/L, b = l/l'$. Each of the integers $j = 1, \ldots, l'$ then defines a value

$$k_j = 2\pi j/L \tag{41}$$

for a cross (24) with arms

$$\boldsymbol{k}_j = (\pm k_j, 0), \quad \boldsymbol{k}_j^{\perp} = (0, \pm k_j) \tag{42}$$

that hosts a tracer configuration with real-valued amplitude f_c. In principle, each choice of inner cutoff parameters $1 \leqslant l' < l$ gives rise to k values $k_1, \ldots, k_{l'}$. In Ref. [18], we have observed strong finite-size irregularities for the correlation function $\tilde{G}(\boldsymbol{k}) = \langle \tilde{f}(\boldsymbol{k}) \tilde{f}(-\boldsymbol{k}) \rangle$ at the smallest accessible nonzero wave vectors, so that it is recommended to exclude the k value k_1 from the following fits. Since one needs a minimum of approximately five to six values to determine dispersions with sufficient statistical reliability (see below), we are confined to lower cutoffs of about $l' \geqslant 6$, which in turn puts an approximate lower limit of $1/b \geqslant 6/l$ on the b values accessible in our simulations. On the other hand, due to the discreteness of the Brillouin zones of our finite systems, the closest accessible value of $1/b$ below its ultimate limit 1.0 is $1/b = (l-1)/l$.

Given such a system, we determine the unnormalized probability distribution $P^{\boldsymbol{k}}(f_c)$ within a certain interval $-f_{\max} \leqslant f_c \leqslant f_{\max}$ by FMC, and thus the dimensionless coarse-grained free energy

$$\tilde{E}^{\boldsymbol{k}}(f_c) := -\ln \frac{P^{\boldsymbol{k}}(f_c)}{P^{\boldsymbol{k}}(0)}. \tag{43}$$

To reliably separate the contributions proportional to f_c^2 from those proportional to f_c^4 in a comparison of (28) to these data requires us to choose a suitable value for $f_{\max}$. To estimate this value, we analyze the bare energy expression (28), assuming that its coarse-grained counterpart will not differ by orders of magnitude from it. After fixing $\kappa \equiv 1$, our only remaining parameter is the value of the remaining bare coupling parameter K. Since both the harmonic as well as the anharmonic contribution to (28) are proportional to k^4, it seems reasonable to choose a common value $f_{\max}$ for the amplitude at which we expect to see a factor of λ between the bare total energy $E^{(c)}$ and its purely harmonic part $E^{(h)}|_{K_N=0}$ uniformly for all k. Numerically, $f_{\max}$ is determined from the equation

$$2\kappa_N f_{\max}^2 + \frac{K_N}{2} f_{\max}^4 \equiv \lambda 2\kappa_N f_{\max}^2, \tag{44}$$

i.e.,

$$f_{\max} = 2N\sqrt{\frac{(\lambda-1)\kappa}{K}}. \tag{45}$$

If λ is chosen too small or too large, it becomes numerically hard to reliably separate harmonic and anharmonic contributions by a least-squares fit. Moreover, the free-energy range that needs to be determined in the simulations increases with growing λ. After performing various numerical tests, we settled for a common factor of $\lambda = 2.6$, which was used in all subsequent simulations. To actually explore the potential shape in this region, a successful simulation approach needs to overcome potentially large free-energy differences. After monitoring the convergence and tunneling properties of several variants of the family of multicanonical algorithms, the $1/t$ variant [36,37] of the Wang-Landau algorithm [38,39] emerged as a robust and reliable choice. Each single simulation was performed with an order of magnitude of 200 tunneling events between $f_c = 0$ and $f_c = f_{\max}$ at the $1/t$ stage, which took about 10^6 single MC sweeps per simulation, and for each value of K that we want to inspect, l' such simulations are needed, one for every k value out of the set $\{k_j : j = 1,2,\ldots,l'\}$. An example of the raw data obtained by such simulations may be inspected in Fig. 1.

The numerical procedure to determine RG recursion relations requires, therefore, a number of nested least-squares fits. On the one hand, the function $\tilde{E}^{\boldsymbol{k}}(f_c)$ obtained from a simulation of the above type will, of course, be contaminated by small contributions of powers higher than f_c^4, i.e., it will not exactly resemble the simple structure of the bare effective Hamiltonian (13). This well-known behavior of generating "new" couplings beyond those present in the original bare Hamiltonian, which is inherent to the RG, can only be dealt with by fitting to a more general ansatz of type

$$\tilde{E}^k(f_c) \equiv a(k) f_c^2 + b(k) f_c^4 + c(k) f_c^6 + d(k) f_c^8 \tag{46}$$

and discarding all coefficients except $a(k)$ and $b(k)$ in the analysis that follows. In a second level of fitting, the resulting collection of coefficients $\{a(\boldsymbol{k}), b(\boldsymbol{k})\}$ is in turn fitted to functions of structure

$$a_{\mathrm{fit}}(k) \equiv 2\tilde{\kappa}_N k^4 + a_6 k^6 + a_8 k^8 + \cdots + a_{n_{\max}} k^{n_{\max}}, \tag{47}$$

$$b_{\mathrm{fit}}(k) \equiv \frac{\tilde{K}_N}{2} k^4 + b_6 k^6 + b_8 k^8 + \cdots + b_{n_{\max}} k^{n_{\max}}, \tag{48}$$

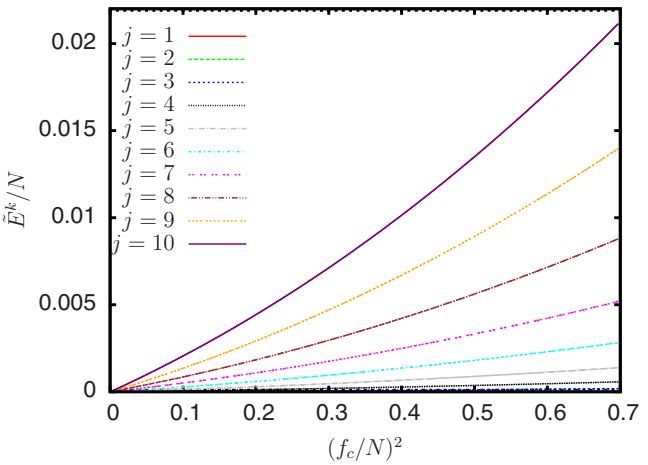

FIG. 1. (Color online) Raw simulation data for systems of size $L = 240$ with outer cutoff $l = 24$, inner cutoff $l' = 10$, and 2D Young modulus $K = 9.16$. Enumerating the displayed lines from bottom to top, the index $j = 1,\ldots,10$ labels the underlying tracer configurations of type (24) with arms (42) parametrized by the wave numbers k_j as defined in Eq. (41).

from which the coarse-grained values $\tilde{\kappa}_N, \tilde{K}_N$ are extracted, while all higher-order fit parameters, which correspond to other higher-order couplings presumably generated by the coarse-graining operation, are ignored once again.

In practice, these fits are not as straightforward to do as it may seem. Our numerical tests did show that for the first level of fitting, using the truncated eight-order polynomial (46) as a fit function order gave numerically convincing results for all considered parameter ranges. However, it turned out to be very hard to decide in advance how to choose the maximum power $n_{\max}$ of k kept in the definition of the fit functions (48) in the second level fitting that aims at extracting the lowest-order $\boldsymbol{k}$ dependence of the functions $a(\boldsymbol{k})$ and $b(\boldsymbol{k})$. Truncating at too low orders may yield a certain tradeoff among the resulting fit parameters and thus adulterate the results. On the other hand, remember that we are necessarily working in a finite system with a discrete Brillouin zone, the minimum spacing between $\boldsymbol{k}$-vector components given by $2\pi/L$, and so only a few data points may be available for low inner cutoff parameter l'. Specifically, for systems with small values of, say, $l' \leqslant 6$, a high-order polynomial fit will not produce meaningful results, since too few unintegrated modes with small $\boldsymbol{k}$ vectors parallel to a chosen direction are at our disposal.

Worse, the importance of higher-order terms in the expansion was observed to strongly vary with the particular value of K chosen. The "optimal" truncation order $n_{\max}$ of the polynomials may thus even depend on K, which makes it very difficult to evaluate the large mass of data generated in our simulations in this way. Worst, it may be difficult to figure out possible "forbidden" powers in the sought-after expansion. For instance, we have explicitly checked numerically that no "surface tension" contribution $\propto k^2$ to $a(k)$ is generated from (17) by the coarse-graining operation, which justifies *a posteriori* the use of (17) as our basic model Hamiltonian. Theoretically, this absence can be contributed to the presence of a Ward identity [see, e.g., the cancellation of k^2 contributions in the sum of contributions to Eqs. (30a)–(30d) of Ref. [25]]. However, it is beyond the scope of the present work to compute all similar constraints on higher-order k-dependent expansion coefficients imposed by Ward identities.

To summarize the above observations, we need to fit data obtained for the collection of $\boldsymbol{k}$ vectors with a function of which only the lowest expansion power is known with certainty. This problem may look hopeless or at least somewhat ill-defined at first glance. Not being aware of any preassembled approach published in the literature on numerical mathematics, we had to come up with our own custom solution. As is explained in more detail in the Appendix, the basic philosophy of our approach is not to focus on the unknown higher-order contributions to the fit functions, but rather to determine the extent of validity of the lowest-order approximation to the underlying data set and reweighting the members of this data set accordingly. Despite currently lacking a rigorous mathematical proof, this seems to work quite well in practice.

Setting $\kappa = 1$ without loss of generality, the above procedure maps every "bare" coupling constant K and shell thickness parameter b into a pair of coarse-grained coupling constants $(\tilde{\kappa}(K), \tilde{K}(K))$. To determine the fixed point K^* of the underlying RG transformation, it is thus necessary to perform simulations for a large number of different K values at each accessible b value to extract the values for the fixed-point coupling $K^*(b)$ and the exponents $\eta(b)$ and $\omega(b)$ for various system sizes. As explained above, for each such K value, this required l' separate Wang-Landau-type simulations (one for each k_j value) to determine the underlying dispersion changes that govern the computation of exponent η. For a numerical study, it is advantageous to switch to a description that is continuous in K, at the same time smoothing the statistical noise contained in the resulting data. To analyze the possible K dependence of $\tilde{\kappa}(K)$ and $\tilde{K}(K)$, we make use of the simple fact that for $K \to 0$ evidently both $\tilde{\kappa}(K) \to \kappa = 1$ and $\tilde{K}(K)/K \to 1$, such that any analytic fit of these functions must start out with value unity at $K = 0$. Otherwise, the only obvious requirement one may impose on a candidate fit function is that it should give a smooth and regular interpolation of the data. Numerical tests have shown that an ansatz of type

$$f(K) = 1 + a\ln(1 + b^2K) + cK + dK^2 + eK^3 \quad (49)$$

with five free parameters $a,\ldots,e$ does a good job in this respect both for $\tilde{\kappa}(K)$ as well as for $\tilde{K}(K)/K$ (cf. Fig. 2 for illustration). With these analytic interpolations at hand, it is now an easy task to carry out the analysis outlined in Eqs. (35)–(40).

Error bars for the numerical quantities derived by these calculations are derived using a corresponding bootstrap analysis [40] based on 100 bootstrap samples drawn from the underlying set of considered coupling values K for each particular choice of (L,l,l').

V. RESULTS

In the present work, we studied three systems with one common value of $\kappa = 1$ and $\Lambda = \pi/5$, with sizes defined by the parameters $(L,l) = (120,12)$, $(240,24)$, and $(360,36)$, respectively. Unfortunately, a complete scan through all

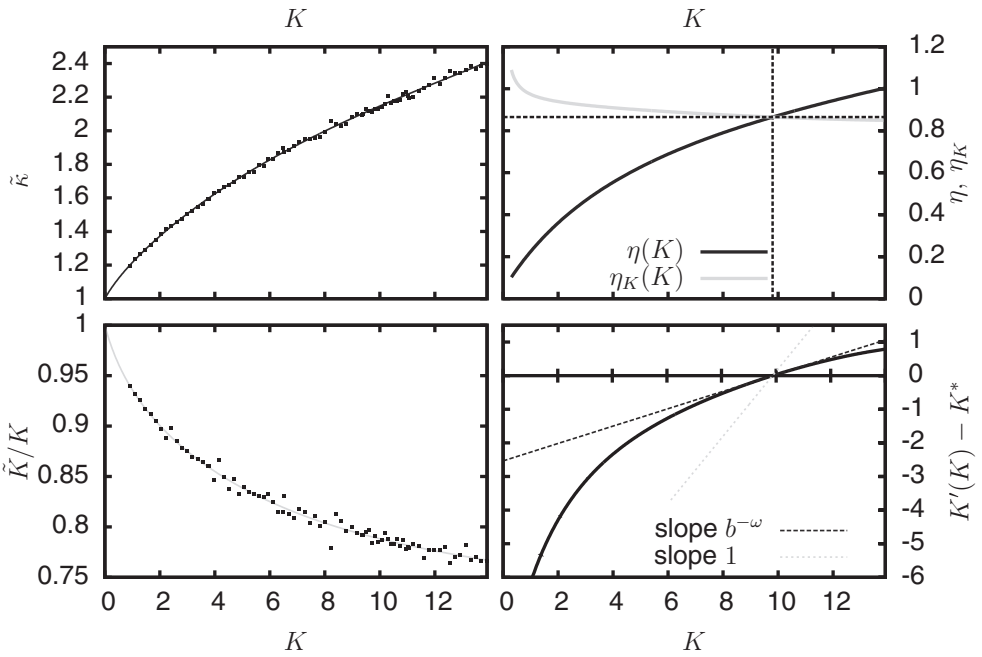

FIG. 2. Illustration of our numerical procedure for parameters $L = 240$, $l = 24$, and $l' = 10$. Left column plots: fits of data for $\tilde{\kappa}(K)$ and $\tilde{K}(K)/K$ to the ansatz (49). Each data point shown is derived from fits of the functions $a(k), b(k)$ based on up to l' different simulation data of the type shown in Fig. 1. Note the excellent compliance of the numerical data with the necessary conditions $\lim_{K\to 0} \tilde{\kappa}(K) = \lim_{K\to 0} \tilde{K}(K)/K = 1$. Right column, upper plot: illustration of the numerical solution of the equations $\eta(K) \equiv \eta_K(K)$ as defined in Eqs. (35) and (36). Right column, lower plot: determination of the slope of function $K'(K) - K^*$ at $K = K^*$. The direction of the RG flow is schematically indicated. In this particular example, the intersection point determined by Eq. (37) is located at $K^* = 9.801\,27$, and we derive exponents $\eta = 0.865\,07$ and $\omega = 1.544\,56$, respectively.

available b values was only possible for the smallest of these systems due to the sheer amount of required computer resources. The resulting fixed-point coupling value $K^*(b)$ for $L = 120$, which is shown in Fig. 3, indicates a monotonous fall throughout the whole accessible range. For $L = 240$, the observed behavior is not in conflict with this hypothesis, and we would be very surprised if the behavior for $L = 360$ were fundamentally different. Thus, it seems reasonable to assume that there is no critical maximum or minimum of $K^*(b)$ throughout the range $0 < 1/b^* < 1$, which only leaves the possibilities $b^* = 1$ or $b^* = \infty$. Give a system defined by (L,l,l'), the one with $l' = l - 1$ is of course one for which $1/b$ is closest to 1. For our present purposes, thin momentum shells have some attractive features. For a thin shell, the number of modes that need to be integrated out during the CG step is rather small, such that the simulations require less CPU time than for thicker shells. At the same time, the large number of remaining unintegrated modes inside the shell should increase the numerical reliability of determining the dispersions $a(k), b(k)$. Unfortunately, however, there is a price to pay for this convenience. In fact, for a thin shell, all values $\tilde{\kappa}(K)$ and $\tilde{K}(K)/K$ were found to be extremely close to 1 over the whole range of considered values of K, which represents a serious challenge to a numerical evaluation. For the larger two systems, the closest accessible estimates for η in this limit are around $\eta \approx 0.93$, which is definitely out of range in comparison to all other published estimates. Although there may exist a common downward trend of $\eta(b)$ for $b \to 1$, it is difficult to estimate the limiting behavior.

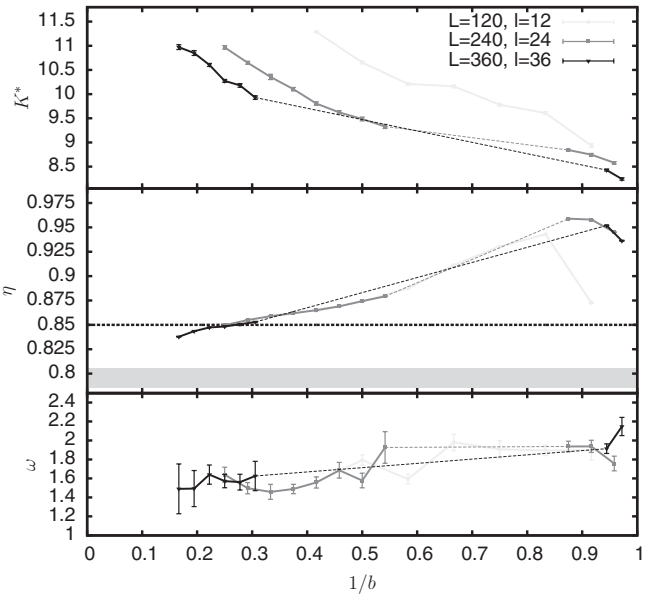

FIG. 3. Numerical results obtained for systems of sizes $L = 120, 240, 360$ with outer cutoff parameters $l = 12, 24, 36$, respectively. Upper plot: b-dependent location $K^*(b)$ of a fixed-point value of parameter K. Middle plot: b-dependent value $\eta(b)$ of exponent η. For comparison, the black dotted horizontal line indicates the functional RG result $\eta = 0.85$, while the horizontal gray bar refers to the FSS estimate of Ref. [18]. Lower plot: b-dependent value $\omega(b)$ of exponent ω.

Turning to the opposite limit $1/b \to 0$, we observe a nice linear decrease of $\eta(b)$ with falling $1/b$, with all the data from various system sizes roughly collapsing on a common same master curve, which indicates that for determining $\eta(b)$, finite-size effects are small to negligible in this limit. Again, it is delicate to extrapolate the data to $1/b \to 0$. If we assumed that the linear trend persists until $1/b \to 0$, we would arrive at a rough estimate of

$$\eta \approx 0.822, \tag{50}$$

which is quite satisfying, as it puts our present calculations roughly in the same ballpark as those done analytically in the framework of the functional RG [23–25], where the estimate $\eta = 0.85$ was derived. Nevertheless, in view of the finite system size used, the imponderables of the above extrapolation $1/b \to 0$, and the fact that even in this limit the residual error due to the influence of irrelevant couplings may only be minimized but not completely eliminated, one clearly should not expect (50) to be equally precise as the estimate $\eta = 0.795(10)$ of Ref. [18] derived from a systematic FSS analysis of the membrane's mean-squared displacement $\langle(\Delta f)^2\rangle$.

Extrapolation of $\omega(b)$ to $b \to \infty$ is also delicate. In fact, to an unprejudiced reader, the data depicted in Fig. 3 will be compatible with at least two scenarios:

(i) Linear extrapolation of $\omega(b)$ to $b \to \infty$ produces a value of roughly $\omega \equiv \lim_{b\to\infty} \omega(b) \approx 4/3 \pm 0.3$.

(ii) The b dependence of $\omega(b)$ may just as well already have saturated for $b \to \infty$ at an asymptotically constant value, leading to any equally crude estimate of $\omega \approx 3/2 \pm 0.3$.

Even though these estimates may not seem to be extremely precise, they pave the way for a considerable further refinement of our previous FSS result, as we show next. To explain this in due detail, let us briefly recapitulate the approach followed in Ref. [18].

The mean-squared displacement $\langle(\Delta f)^2\rangle$ is expected to exhibit a finite-size scaling behavior of type

$$\langle(\Delta f)^2\rangle \sim \delta + \alpha L^{2-\eta}\,[1 + \zeta(L)]\,. \tag{51}$$

The main obstacle to overcome in an attempt to determine the exponent η with high precision is to assess the factor $\zeta(L)$ that hosts the subleading corrections to scaling by constructing an appropriate ansatz. In principle, these corrections arise from the presence of irrelevant couplings, and thus the leading contributions to $\zeta(L)$ should correspond to powers of $1/L^{\omega}, 1/L^{\omega_2}, \ldots$, where ω_2 denotes the Wegner exponent of the next-to-leading irrelevant coupling [41,42] [in Ref. [18], an additional logarithmic contribution of type $\zeta(L) = \beta \ln L + \gamma/L^{\omega} + \cdots$ has already been ruled out]. Unfortunately, however, we had (and have) been unable to spot any published numerical estimate for the correction to scaling exponent ω in the literature. Interestingly, while such an estimate may have been beyond reach for previous simulation approaches to the flat phase of tethered membranes, it seems as if ω is equally hard to extract from analytical methods [28]. Lacking any estimate of the correction to scaling exponent ω, in Ref. [18] we had chosen to monitor the error bars for the remaining fit parameters produced by different choices of ω in the interval $[0,1]$. Based on this reasoning, the estimate $\eta = 0.795(10)$ of Ref. [18] quoted above had finally been derived for the "naive" choice $\zeta(L) = \beta/L + \gamma/L^2$. Unfortunately, however, the sign of the resulting value δ produced in this fit is positive, a fact that was not given much attention in Ref. [18]. Recall that according to Eq. (5) of Ref. [18]

$$\langle(\Delta f)^2\rangle \sim \int \frac{d^2q}{(2\pi)^2}\tilde{G}(\boldsymbol{q}), \tag{52}$$

where asymptotically for $|\boldsymbol{q}| \to \boldsymbol{0}$

$$\tilde{G}(\boldsymbol{q}) = \langle|\tilde{f}(\boldsymbol{q})|^2\rangle \sim \frac{1}{\kappa q^{4-\eta}}. \tag{53}$$

Based on this ideal power law, a spherical cutoff geometry $2\pi/L \leqslant |\boldsymbol{q}| \leqslant \Lambda$ results in

$$(\Delta f)^2 \sim \int_{2\pi/L}^{\Lambda} \frac{dk/(2\pi)^2}{\kappa k^{3-\eta}} = \frac{-\Lambda^{2-\eta} + (L/2\pi)^{2-\eta}}{(2\pi)^2(2-\eta)\kappa}, \tag{54}$$

which implies a *negative* value $\delta = -\Lambda^{2-\eta}/(2\pi)^2(2-\eta)\kappa$, and it is reasonable to expect that this heuristic observation also carries over to the case of cubic cutoff geometry with subleading scaling corrections included.

Our present RG approach, in which $\omega(b)$ is derived in (40) as a by-product of locating the FP coupling $K^*(b)$ and the exponent $\eta(b)$ without extra effort, now puts us in a position to shed some new light on these problems, even though some residual speculations on the structure of $\zeta(L)$ are still involved. We propose the ansatz [5,41–44]

$$\zeta(L) = \beta/L^{\omega} + \gamma/L^{2\omega} + \cdots, \tag{55}$$

which amounts to assuming that either $\omega_2 \approx 2\omega$ or $\omega_2 \gg 2\omega$, and also to completely discarding additional "analytic" corrections of type $1/L$. While the first assumption is admittedly difficult to justify based on our present knowledge, the latter appears to be reasonable for periodic boundary conditions where the renormalization of the scaling field $g_L = 1/L$ is trivial [45]. To evaluate the impact of these scenarios on the numerical estimate of η, we have carried out new fits of the FSS ansatz (51) for various choices $0.6 \leqslant \omega \leqslant 2.0$ to the data for $\langle(\Delta f)^2\rangle$ generated in Ref. [18]. The results, which are shown in Fig. 4, reveal a number of interesting points.

According to Fig. 4, $\delta < 0$ appears to hold only for ω somewhat larger than $2 - \eta \approx 1.22$, a range of values for ω that had unfortunately not been considered in Ref. [18]. Our fits obviously become singular near this value, but this should not come as a surprise: quite trivially, for ω equal to $2 - \eta$, multiplication of the correction β/L^{ω} in (55) with $L^{2-\eta}$ produces yet another constant besides δ, which results in an ill-defined fitting prescription in the close vicinity of this value of ω. As the top left plot of Fig. 4 indicates, for both our two possible extrapolations $\omega = 4/3$ and $3/2$, the parameter δ is indeed negative. We obtain

$$\eta = \begin{cases} 0.7935(34), & \omega = 4/3, \\ 0.7927(29), & \omega = 3/2. \end{cases} \tag{56}$$

The accompanying goodness-of-fit parameter Q [46] displays a minimum near $\omega = 3/2$ (cf. the top right plot of Fig. 4), thus slightly favoring the second of the two scenarios (56). In retrospect, we note that their common denominator, namely the assertion $\omega > 1$, could have been already anticipated from

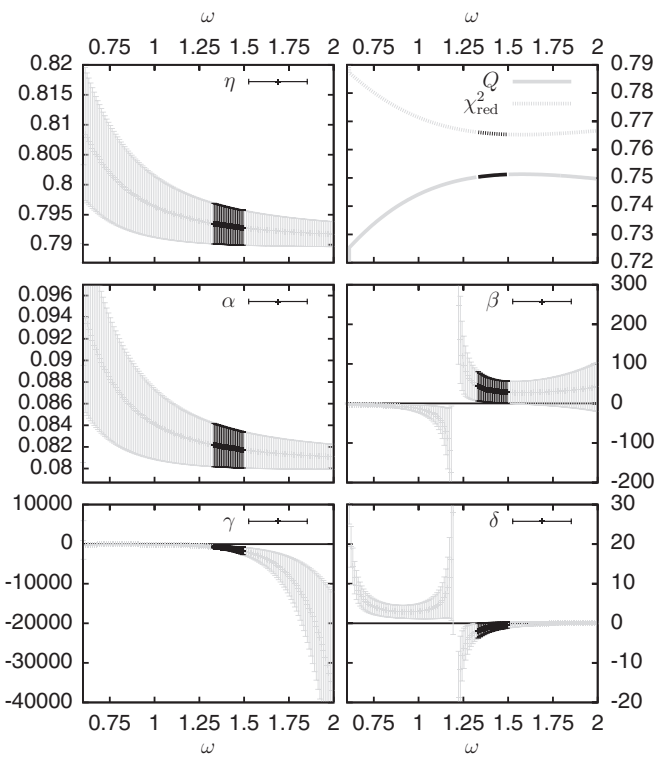

FIG. 4. Results of least-squares fits of the ansatz (51) to the data for $\langle(\Delta f)^2\rangle$ obtained in Ref. [18] for various choices $0.6 \leqslant \omega \leqslant 2.0$. Data not within the range $4/3 \leqslant \omega \leqslant 3/2$ are plotted in gray as a guide to the eye. Top left panel: fit results for η. Top right panel: ω dependence of goodness-of-fit parameter Q and reduced χ^2 parameter of the fits. Bottom right panel: ω dependence of fit parameter δ. Note the discontinuous change of sign around $\omega \approx 1.22$. Remaining panels: ω dependence of other fit parameters α, β, and γ.

a FSS analysis similar to the carried out in Ref. [18] if only we had monitored the sign of the resulting fit parameter δ in the ansatz (51) for $\langle(\Delta f)^2\rangle$.

In closing this section, we note that our asymptotic fitting procedure, which we have used above to compute coarse-grained parameters and which is explained in the Appendix, offers a complementary way to estimate η from the FSS of $\langle(\Delta f)^2\rangle$. After all, it was designed for the very purpose of extracting leading functional dependencies from data with unknown higher-order corrections. Based on application of the linear ansatz $\log\langle(\Delta f)^2\rangle \sim \log\alpha + (2-\eta)\log L$ to the logarithms of the data points, the result $\eta = 0.7948$ obtained by our simple recipe is impressively close to that of our above elaborate FSS analysis, with nothing more than the leading scaling behavior as input, even though it may be difficult to estimate the corresponding error bar.

VI. DISCUSSION AND OUTLOOK

In this paper, we have illustrated the practical feasibility and usefulness of our FMC implementation of Wilson's MSRG for the flat phase of a crystalline membrane, a nontrivial model of continuing physical interest. In particular, we have demonstrated the ability of our method to derive the—albeit crude—numerical estimate $\omega \pm 0.3 \in [4/3,3/2]$ for the correction to a scaling exponent in a situation in which all other approaches have failed so far. However, for a meaningful numerical analysis, it is mandatory to monitor the dependence of observables on the thickness parameter b of the employed momentum shell.

Our RG result for ω also allowed us to construct an improved FSS procedure for $\langle(\Delta f)^2\rangle$. The resulting estimates (56) for the exponent η deviate even more from the value $\eta = 0.85$ derived from functional RG [23–25] than our previous one $\eta = 0.795(10)$ given in Ref. [18]. In fact, they happen to be much closer to the result $\eta = 0.78\,22(5)$ extracted from a second-order self-consistent screening approximation [20]. On the other hand, even our own RG results (50) for η show a similar tendency to exceed the FSS estimates. A heuristic explanation for this common tendency of RG approaches to overestimate η is as follows.

For the flat membrane model, Fig. 3 indicates that the influence of irrelevant couplings is minimal for $b \to \infty$. Still, even in this limit our RG estimate (50) is noticeably higher than all those obtained from FSS, no matter which kind of scaling corrections we employ, even though the underlying data were generated using the same underlying FMC algorithm. As Fig. 3 indicates, our RG analysis seems not to be afflicted with appreciable finite-size effects. Thus, the only explanation for this discrepancy is a residual bias of the RG result due to the influence of the irrelevant couplings that survives the limit $b \to \infty$. In fact, had we not been carefully monitoring the b dependence of our results but had simply chosen one particularly convenient shell configuration, our result for η might have been still dramatically higher, as the middle panel of Fig. 3 indicates. In view of the fact that generic functional RG calculations also include choosing a projection to a low-dimensional coupling constant space and a cutoff function, these observations may hint at the source of the persistent discrepancy between RG and FSS estimates for η.

In the near future, we plan to investigate the critical behavior of hexatic membranes in the so-called crinkled phase [47–50] using a similar strategy. Compared to that of crystalline membranes, this problem is closely related but technically much more involved due to the fact that for hexatic membranes, a surface tension contribution of type

$$\mathcal{H}^{\Lambda,s} = \mu \int \frac{d^2q}{(2\pi)^2} q^2 |\tilde{f}(\boldsymbol{q})|^2 \tag{57}$$

has to be taken into account, its coupling constant μ being relevant in the RG sense [50]. Using conventional FMC, we have found it very difficult to determine the critical value $\mu_c^*(\kappa)$ to which μ must be tuned at a given value of κ to actually observe the crinkled phase [51]. Our present approach offers a way to do this, but at the expense of determining a two-dimensional flow pattern in the variables κ and μ at fixed parameter K. Work in this direction is currently in progress.

ACKNOWLEDGMENTS

We appreciate valuable advice from M. Hasenbusch concerning our finite-size scaling approach. We acknowledge support by the Austrian Science Fund (FWF) Project P22087-N16. Major parts of our computations were performed on the Vienna Scientific Cluster (VSC1 and VSC2).

APPENDIX

To demonstrate the fitting strategy used in extracting the lowest-order dispersion coefficients from the functions $a(k)$ and $b(k)$, we consider a simple toy model defined by the function

$$f(x) = 0.09x^2 - 0.1x^4 - 0.2x^6 + 0.9x^8 \qquad \text{(A1)}$$

in the interval $[0,1]$. We choose the 20 equidistant points $x_n := 0.05n$, $n = 1, \ldots 20$ from this interval, and we generate the telescopic data sets

$$F_k := \{(x_n, f(x_n)) : n = 1, \ldots, k\},\ k = 1, \ldots, 20\,. \qquad \text{(A2)}$$

We will use the largest considered data set F_{20} holding 20 function values as the input data to our procedure, whose goal it is to reconstruct the leading coefficient 0.09 of $f(x)$, based only on the information that $f(x)$ should start out with a term $\propto x^2$ multiplied by a non-negative coefficient.

We start by choosing the fit function

$$\varphi(x) := a^2 x^2, \qquad \text{(A3)}$$

which deliberately ignores all higher-order corrections to this leading x dependence that should gradually kick in for growing values of x. Of course, the quality of a series of least-squares fits of this function applied to the sets F_k will successively degrade with growing k. Quantitatively, we will observe a crossover from a slow to a steep rise of the accompanying χ^2 parameters,

$$\chi_k^2 := \sum_{l=1}^{k} [f(x_l) - \varphi(x_l)]^2, \quad k = 1, \ldots, 20, \qquad \text{(A4)}$$

with growing k. The idea is to use the inverse values

$$w_k := \begin{cases} 1/\chi_2^2, & k \leqslant 2, \\ 1/\chi_k^2, & k > 2 \end{cases} \qquad \text{(A5)}$$

[since trivially χ_1^2 should vanish, we have put $w_1 \equiv w_2$ in (A5)] as statistical weights for the data points $(x_n, f(x_n))$ in a final least-squares fit of (A3) to the full data set F_{20}, which produces our final estimate for a^2.

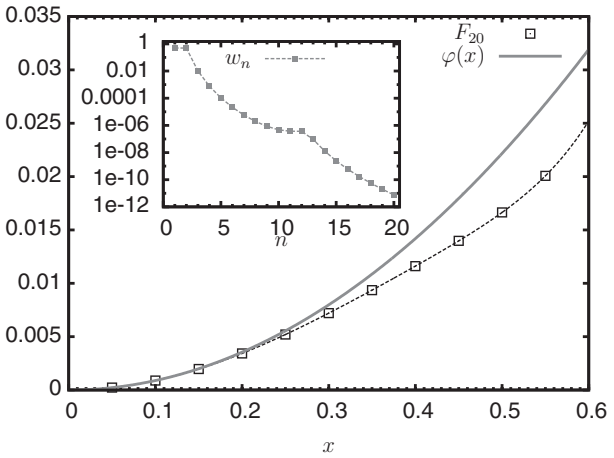

FIG. 5. Illustration of the fit procedure outlined in Eqs. (A1)–(A5). Main plot: original data set F_{20} produced from the function (A1) and final fit with Eq. (A3) [but only shown in the interval (0,0.6)]. Inset: normalized weights obtained for all 20 data points of the data set F_{20} (note the logarithmic scale).

The described procedure is simple to implement and robust, but, of course, far from perfect. Obviously, its success relies on the high quality of the underlying data. In particular, it is vulnerable to statistical outliers located inside the asymptotic region $x \ll 1$. Nevertheless, at least in the context of the present paper, where the unknown higher-order correction terms can be expected to be small compared to the leading term, it seems to produce sufficiently accurate results. For example, in the case of the toy function (A1), we obtain $a = 0.297\,81$, which is within 0.73% of the exact value $0.3 = \sqrt{0.09}$. In view of the fact that we did not have to make any assumptions on the structure of the fitting function beyond its lowest-order term, the achieved precision is quite satisfactory. Figure 5 illustrates the resulting final fit of $\varphi(x)$ to the full data set F_{20} obtained by reweighting its data using the weights w_k successively generated by the previous fits to the data sets F_k.

[1] K. G. Wilson, Rev. Mod. Phys. **55**, 583 (1983).
[2] J. Zinn-Justin, *Quantum Field Theory and Critical Phenomena* (Oxford University Press, Oxford, 2002).
[3] H. Kleinert and V. Schulte-Frohlinde, *Critical Properties of ϕ^4-Theories* (World Scientific, Singapore, 2001).
[4] P. Kopietz, L. Bartosch, and F. Schütz, *Introduction to the Functional Renormalization Group* (Springer, Berlin, 2010).
[5] D. Amit and V. Martin-Mayor, *Field Theory, the Renormalization Group, and Critical Phenomena: Graphs to Computers*, 3rd ed. (World Scientific, Singapore, 2005).
[6] D. Landau and K. Binder, *A Guide to Monte Carlo Simulations in Statistical Physics*, 3rd ed. (Cambridge University Press, Cambridge, 2009).
[7] A. Tröster, Phys. Rev. B **76**, 012402 (2007).
[8] A. Tröster and C. Dellago, Phys. Proc. **6**, 106 (2010).
[9] A. Tröster, Phys. Rev. Lett. **100**, 140602 (2008).
[10] A. Tröster, Comput. Phys. Commun. **179**, 30 (2008).
[11] A. Tröster, Phys. Rev. B **81**, 012406 (2010).
[12] A. Tröster, Phys. Rev. E **79**, 036707 (2009).
[13] A. Tröster, Comput. Phys. Commun. **182**, 1837 (2011).
[14] A. Bruce, M. Droz, and A. Aharony, J. Phys. C **7**, 3673 (1974).
[15] A. Tröster, Phys. Rev. B **81**, 125135 (2010).
[16] M. Fisher, S. Ma, and B. Nickel, Phys. Rev. Lett. **29**, 917 (1972).
[17] *Statistical Mechanics of Membranes and Surfaces*, edited by D. Nelson, T. Piran, and S. Weinberg (World Scientific, Singapore, 1988).
[18] A. Tröster, Phys. Rev. B **87**, 104112 (2013).
[19] P. Le Doussal and L. Radzihovsky, Phys. Rev. Lett. **69**, 1209 (1992).
[20] D. Gazit, Phys. Rev. E **80**, 041117 (2009).
[21] J. A. Aronovitz and T. C. Lubensky, Phys. Rev. Lett. **60**, 2634 (1988).
[22] F. David and E. Guitter, Europhys. Lett. **5**, 709 (1988).
[23] J.-P. Kownacki and D. Mouhanna, Phys. Rev. E **79**, 040101 (2009).

[24] F. L. Braghin and N. Hasselmann, Phys. Rev. B **82**, 035407 (2010).
[25] N. Hasselmann and F. L. Braghin, Phys. Rev. E **83**, 031137 (2011).
[26] M. J. Bowick, S. M. Catterall, M. Falcioni, G. Thorleifsson, and K. N. Anagnostopoulos, J. Phys. I **6**, 1321 (1996).
[27] J. H. Los, M. I. Katsnelson, O. V. Yazyev, K. V. Zakharchenko, and A. Fasolino, Phys. Rev. B **80**, 121405(R) (2009).
[28] J. K. Wiese, *Polymerized Membranes, a Review*, in *Phase Transitions and Critical Phenomena*, edited by C. Domb and J. Lebowitz (Academic, London, 2000).
[29] H. Kleinert, *Path Integrals in Quantum Mechanics, Statistics, Polymer Physics, and Financial Markets* (World Scientific, Singapore, 2009).
[30] E. Luijten, Ph.D. thesis, Delft University of Technology, The Netherlands, 1997.
[31] S. A. Safran, *Statistical Thermodynamics of Surfaces, Interfaces, and Membranes* (Perseus Books, Cambridge, MA, 2003).
[32] M. I. Katsnelson, *Graphene: Carbon in Two Dimensions* (Cambridge University Press, Cambridge, UK, 2012).
[33] A. Tröster and C. Dellago, Ferroelectrics **354**, 225 (2007).
[34] A. Tröster, Phys. Proc. **53**, 96 (2014).
[35] F. J. Wegner, Phys. Rev. B **5**, 4529 (1972).
[36] R. E. Belardinelli and V. D. Pereyra, J. Chem. Phys. **127**, 184105 (2007).
[37] R. E. Belardinelli, S. Manzi, and V. D. Pereyra, Phys. Rev. E **78**, 067701 (2008).
[38] F. Wang and D. P. Landau, Phys. Rev. Lett. **86**, 2050 (2001).
[39] D. P. Landau and F. Wang, Braz. J. Phys. **34**, 354 (2004).
[40] B. Efron and R. Tibshirani, *An Introduction to the Bootstrap* (Chapman and Hall, Boca Raton, FL, 1994).
[41] M. Barber, in *Phase Transitions and Critical Phenomena*, edited by C. Domb and J. Lebowitz (Academic, New York, 1983), Chap. 2, p. 145.
[42] V. Privman, *Finite Size Scaling and Numerical Simulation of Statistical Systems* (World Scientific, Singapore, 1990).
[43] A. Pelissetto and E. Vicari, Phys. Rep. **368**, 549 (2002).
[44] M. Hasenbusch, Phys. Rev. B **82**, 174433 (2010).
[45] J. Salas and A. D. Sokal, J. Stat. Phys. **98**, 551 (2000); see also arXiv:cond-mat/9904038.
[46] W. H. Press, S. A. Teukolsky, W. T. Vetterling, and B. P. Flannery, *Numerical Recipes: The Art of Scientific Computing*, 3rd ed. (Cambridge University Press, Cambridge, UK, 2007).
[47] F. David, E. Guitter, and L. Peliti, J. Phys. (Paris) **48**, 2059 (1987).
[48] M. Bowick and A. Travesset, Phys. Rep. **344**, 255 (2001).
[49] E. Guitter and M. Kardar, Europhys. Lett. **13**, 441 (1990).
[50] A. Codello and O. Zanusso, Phys. Rev. E **88**, 022135 (2013).
[51] A. Tröster, J. Phys.: Conf. Ser. **510**, 012008 (2014).